Photogrammetric Evaluation of Shear Modulus of Glulam Timber Using Torsion Test Method and Dual Stereo Vision System

Ahmed Mohamed
Edinburgh Napier University
Yu Deng
Guangxi University of Science and Technology
Hexin Zhang (j.zhang@napier.ac.uk)
Edinburgh Napier University
Simon H F Wong
Technological Higher Education Institute of Hong Kong
Kal Uheida
Edinburgh Napier University
Y.X. Zhang
Shanghai Normal University
Martin Lehmann
Bern University of Applied Sciences
Yanfang Quan
Guangxi University of Science and Technology

Research Article

Keywords: timber glulam beams, shear modulus, torsion, photogrammetry, stereo vision techniques

Posted Date: June 16th, 2021

DOI: https://doi.org/10.21203/rs.3.rs-622610/v1

Abstract

The shear modulus of timber and timber-based composite materials is a fundamental mechanical property which is used in the design of timber and engineered wood products. The problem of experimentally determining appropriate values of shear modulus for timber-based composite is not as simple and straightforward as in isotropic materials. Although the torsion test is a recommended standard approach to determine the shear modulus of structural-size timber and glulam beams, it is a difficult to measure the rotational deformations of the timber beams. Therefore, in this paper, a stereo camera system combined with a photogrammetric approach is proposed to evaluate the values and variations of the shear modulus of glulam beams under the torsion test. The photogrammetric approach is a non-contact method which provides an efficient and alternative approach for measuring the deformations of the torsion specimens in three dimensions. A series of experiments were conducted on glulam timber beams under the torsion test to investigate the applicability of the optical approach to evaluate the values and variations of shear modulus as well as to investigate the effect of applying torques in a clockwise or anticlockwise direction on the shear modulus of the beams. This optical system not only allows the performance and reliability of the traditional sensors to be assessed, but also allows the rotational deformation of the torsion samples to be monitored at various locations. This enables the values of shear modulus at different cross-sections of the torsion specimens to be evaluated without the need to use more devices. The test results showed that applying torques to the glulam timber specimens during loading and unloading in either a clockwise or anticlockwise direction does not influence or cause a significant change in the shear modulus of the beams. By comparing shear modulus values of glulam beams measured based on different shear spans, it was found that the larger the shear span the smaller the shear modulus value. This might indicate that the variations of shear modulus values at these different gauge lengths needs to be considered.

Introduction

The shear modulus of produced timber and timber-based composite beams is of considerable importance as it plays a very significant role in structural modelling, such as the lateral torsional stability of beams (EN 1995-1-1, 2004), and designing serviceability of wood- beam floors (Foschi, 1982). It is also an important input for developing analytical and finite element models (Chui, 2002, Jiang et al., 2004). The torsion test provides a state of pure shear stress distribution in the specimen (Hindman et al., 2005, Gharavi et al., 2018, Gharavi and Zhang, 2018, Gharavi, et al. 2017), allowing measurement of the pure shear properties. This method is considered to be a suitable approach for determining the shear modulus of timber and timber-based composite materials. The most recently updated British Standard, BS EN 408:2012 recommended the torsion test as a standard approach to determine the shear modulus of structural-size timber and glulam beams. Recently, the torsion test has been adopted by more and more researchers (including Gupta et al., 2002, Gupta, 2005, Hindman et al., 2005, Khokhar et al., 2009, Khokhar et al., 2010, Zhang et al., 2011, Zhang et al., 2012) to evaluate the shear modulus of structural-size timber and glulam beams.

In the torsion test, the exact measurement of the relative angle of twist over a gauge length is essential to determine the shear strain and hence enable the calculation of shear modulus. The rotations measured by the torsion tester machines, such as the Tinius Olsen machine, may include small slippage between the board and the clamps of the testing machine. To overcome this difficulty, angle measurement devices, such as inclinometers, are traditionally used to measure the rotations of the torsion specimens. Although this mechanical device has proven to be accurate and flexible for measuring the rotations, it presents some significant drawbacks. Configuring the sensor tends to be time-consuming and labour intensive and it can be damaged or destroyed during destructive testing. The size of this sensor and the nature of the surface contact it is measuring have prevented it from being used to measure more details of the shear deformations, details which might help to evaluate the variations of shear modulus (G) of timber and glulam beams. The photogrammetric approach is proposed in this research to measure the surface rotations of the torsion samples.

Monitoring tools using photogrammetry and image processing have been used in timber to measure mechanical properties, 3D displacements, or deformations at various points of the same specimen, as proposed in various experiments (Choi et al., 1991, Dahl and Malo, 2009a, Dahl and Malo, 2009b, Franke et al., 2007, Garcia and Orteu, 2001, Maas and Hampel, 2006, Guindos and Ortiz, 2012, Xavier et al., 2012, and). In contrast to the traditional techniques, the photogrammetric approach could provide more details of angular deformation which are necessary for providing more details of shear deformation of torsion specimens. It provides a permanent visual and measurement record for further assessment. Optical methods that give displacements or strain fields are now widely used to evaluate material properties of timber-based composite. However, most of these methods have been extremely limited to give in-plane measurements, meaning that the results are not fully applicable to real structural systems.

This paper presents the experimental studies performed to investigate the feasibility of the developed photogrammetric system on the torsion test. Torsion tests were conducted on glulam timber beams according to the EN 408:2012 procedure of the standard torsion tests. The main purpose of this study is to provide an effective alternative method for evaluating the values and the variation of the shear modulus of glulam beams. Another objective of this study was to evaluate torsional behaviour of glulam timber beams and to investigate the effect of shear spans on the values of shear modulus. This may assist in understanding the torsional behaviour of the specimens and give a basis for further studies.

Shear Modulus From Torsion Test

The torsion test method has been included in the most recently updated British Standard, BS EN 408:2010+A1:2012 to obtain the shear modulus of timber. As described in the standard, the relative rotational displacements and the torque must be measured at two sections, which are spaced within the free testing length. Based on the Saint-Venant torsion theory of rectangular cross-section, the value of the shear modulus for each torsion specimen (G_{Tor}) can be calculated using the equation given in EN 408:2012: **see formula 1 in the supplementary files.**

where l_1 is the gauge length and K_{Tor} is the torque stiffness, which can be determined using a linear regression analysis conducted on the linear elastic portion of the graph of applied torque within proportional limits and relative twist of the specimen. *h* and *b* are the depth and width of the specimen, respectively. η is a shape factor, which depends on the depth to width ratio and can be determined from a Table given in (EN 408:2012).

Materials And Methods

The rectangular cross-section timber glulam beams used in this study as samples for the torsion tests had cross sectional dimensions of about 45 mm x 220 mm and the total length of each beam was about 4 meters, as shown in Fig. 1 (a). These beams are graded to GL24 class strength. This grade of glulam beams was selected because it is common and regularly available in the UK. As described in EN 408 (2012) standard, the glulam samples were stored in a conditioning room with a constant temperature of 20^{O} C and a relative humidity of 65%.

Before testing and in order to employ the stereo camera systems for actual angular measurements, the glulam timber beams were prepared by applying photogrammetric targets to their surfaces. This was achieved by painting the area of interest with a white paint to serve as a background which can assist in distinguishing the targets during image processing. Then, black circular marks (targets) were painted on the background. These targets are used to measure the rotations along the depth of the test specimen. Circular marks are preferred because their centre point can be determined with high accuracy (Steger et al., 2008). The photogrammetric patterns consist of 121 circular targets arranged in 11 columns and 11 rows. These targets were marked 20 mm centre to centre to give traceable marks on the sample surfaces. The radius of the circular targets is 10 mm and the central target was set to be an origin of the X-Y coordinate system. Fig. 1 (a) shows an image of these glulam beams. In order to calculate the cross-sectional rotation, a straight cross-sectional reference line was linearly fitted from the 11 coordinates measured for each column. All the glulam samples after being prepared with the photogrammetric targets are shown in Fig. 1 (b).

A Tinius-Olsen (Tinius Olsen, Pennsylvania USA) torsion testing machine capable of applying up to 1 kilo newton-metre (kN-m) torque was used to perform the torsion tests on the specimens. Inclinometers (Model IS-2-30, Level Developments, UK) were employed to measure the angles of twist of the glulam beams at the attached points. The IS-2-30 is a dual axis sensor capable of measuring angles with a measurement range of ±30° in two directions with an accuracy of ± 0.05°. The diameter of the circular base is 43mm. These inclinometers can measure the relative twist angle in both X and Y directions. A data log interface, as shown in Fig. 2, was developed by the authors of this study to simultaneously display, record and transfer data received from the inclinometers to a desktop computer, depending on the time interval specified by the user of the system.

In addition to inclinometers, two binocular stereo camera systems, as shown in Fig. 3 (a), were used to measure the actual rotational deformations of the long side of the cross section of the glulam

specimens. Each of these sensors consists of two DMK 23GP031 cameras with a total resolution of 2592 x 1944 pixels and high-speed CMOS area scan sensor. These cameras were fitted with an Azure-3514M5M lens having a constant focal length of 35 mm and pixel size of 2.2 microns. Additionally, two LED light sources were employed to assist in providing a homogenous illumination of the stereo images. To capture the rotational deformations of the targets in real time, the authors of this research implemented MFC-based application, which was developed based on visual C++ 2010, providing the functions necessary to calibrate the binocular system and to record the image data during testing. The graphical user interface (GUI) of the developed application, as shown in Fig. 3 (b), makes use of libraries included in the image processing software, HALCON (MVTech Software HALCON GmbH., 2010). These include functions not only for calibrating the binocular stereo system easily and accurately but also for 3-dimensional image photogrammetry.

Experimental Setup And Procedure

Fig. 4 shows a schematic of the components of the torsion test setup and an image of this experimental setup is shown in Fig. 5. The glulam specimen was inserted in the torsion machine and four inclinometers were attached to the upper surface of the torsion sample. For validation purposes, inclinometers B and C were placed exactly above the photogrammetric patterns. The stereo cameras, Basler Pilot piA2400-17gm camera, 5M pixel, Monochrome 2/3” CCD with GigE fast Ethernet interface, were mounted on a tripod and the baseline distance was set at about 25cm. The width and heigh of a cell on the CCD-chip are all $2.2x10^{-3}$ mm. The two stereo camera systems were placed in front of the left and right photogrammetric pattern, respectively at a distance around 2.5m away from the beam. The LED light sources were focused on the region of interest to negate the influence of natural and indoor lighting and to provide a homogenous illumination of the torsion sample. Prior to all torsional tests, the two camera systems were calibrated using a 100 mm x100 mm calibration plate and based on the stereo camera calibration of HALCON. The standard calibration plate was chosen according to the estimated dimensions of the region of interest to be captured as described in (MVTech Software HALCON GmbH., 2019). This target consists of 49 marks whose 3D coordinates are known with a high accuracy. The coordinates of these targets are given in the calibration description file which is available according to the dimension of the calibration plate as mentioned in (MVTech Software HALCON GmbH., 2019). More information about the calibration of the stereo cameras is given in detail in Steger et al. (2008). Once the binocular stereo systems were calibrated, the torsion tests were carried out four times for each torsion specimen according to the [1] procedure of the standard torsion tests.

Preliminary torsion tests were carried out on the first sample to determine the rate of loading and to estimate the elastic range of the sample in order to ensure that no permanent deformation occurred during testing under torsional loading. Each sample was tested in the same manner; by applying a torque to the specimen, in the clockwise direction within the elastic range, at a constant rate of twist equal to five degrees per minute both in loading and unloading until the torsion angle of the tester reached 15°. The

direction of the torsion torque was then reversed to an anticlockwise direction with the same loading rate until the torsion angle of the tester reached 15°. Finally, the loading chuck was then returned to its initial test position to allow the test specimen to be removed from the machine. During the torque application, the implemented software was automated to record stereo images of the two regions of interest of the sample at a time interval of 5 seconds. The implemented GUI developed for the inclinometers was also employed to record their reading during the period of the test.

Experimental Results And Discussion

5.1 Calibration Results of the Stereo Camera Systems

In order to reconstruct the 3D coordinates of the photogrammetric targets captured by the stereo cameras, and hence determine their rotational deformations, the calibration parameters of the stereo camera systems were determined by performing the binocular stereo camera calibration of each system using the image processing software. This was achieved via a least square solution with suitable chosen parameters of the cameras that can be determined from the specification of the camera sensor and lens. Tables 1 and 2 show selected examples of the internal and external parameters, including the rotation angles and the translation vector determined from the first stereo system. A screenshot of the developed GUI during the process of calibrating the stereo camera system is shown in Fig. 6.

5.2 Target Tracking and 3D Reconstruction

The image processing algorithm is based on the comparison between two images acquired during the test, one before and after deformation. Fig. 7 demonstrates the concept and steps involved in the algorithm. The process starts with reading the calibration files and displaying the stereo images of the targets recorded from the left and right cameras during testing. Based on their shape and size, the potential targets were determined and tracked from the two sequences of stereo images using the sub pixel-precise segmentation method. These targets were fitted to ellipse shapes and their image coordinates in both the left and right images were measured. The 3D coordinates of the targets expressed in the camera coordinates of the left camera were determined using the theory of triangulation [2]. These coordinates were then used in the calculation of the displacements and rotations of the targets during the period of tests. This was achieved by finding the pixel coordinates of the targets of each pattern and averaging these values to define a point with the average pixel coordinates of the pattern. The pixel coordinates of the other two points were determined for each pair of the stereo images by processing the initial images before applying torque to the specimens. Utilizing the calibration parameters of the stereo camera system and triangulation, the 3D coordinates of the three points were determined to define two vectors. Using the two vectors, the rotations of the photogrammetric patterns for each time interval were then calculated.

5.3 Comparison of Angular Deformations Measured by Inclinometers and the Photogrammetric Systems

To understand the differences between the rotations of the long and short sides of the cross section, the rotations of photogrammetric patterns 1 and 2 and the rotations of inclinometers B and C were plotted in the same figure. These data were measured in both clockwise and anticlockwise directions under torque loading and unloading phases. Fig. 8 (a) and (b) show some selected examples of these comparisons and indicate remarkable results. It is evident that a good agreement between the two methods has been observed and this indicates that the measurements of the rotations of the short side with inclinometers are acceptable.

To investigate the correlation between the measurements, the rotation results of the inclinometers and stereo camera systems were plotted against each other and a very strong correlation was observed for each glulam timber specimen. Selected examples of this comparison are shown in Fig. 9 (a) and (b) in which the rotations of specimen 4, measured in the torsional direction by inclinometers B and C and by the first and second binocular stereo systems, were plotted against each other. These figures provide further evidence of this correlation when considering the correlation of determination (R^2) of the angular measurements of inclinometers versus stereo camera systems. From the results shown in these figures a high degree of correlation, with an R-squared value of 0.999, was observed.

5.4 Torsional Behaviour of the Glulam Timber Beams

The results of preliminary tests that were carried out on specimen 1 revealed that the maximum torque applied to the specimen was within the linear-elastic range, about 250 N.m, and the torsion specimen could be twisted by up to 15° before it began to behave non-linearly. This result was found from the inclinometers which were mounted near the reactional supports. Based on this finding, torsion tests were conducted four times on each of the remaining eleven specimens (2-12) under cyclic loading in the clockwise and anticlockwise directions. The recorded torques measured from the torque cell of the torsion machine, were analyses and displayed graphically. As an example, the torque versus time graph obtained from the first torsion test conducted on glulam specimen 2 under loading and unloading phases is shown in Fig. 10. This plot indicates that the relationship between the values of torque and the corresponding time is approximately linear during the different phases of loadings, confirming that the torsion specimen was within the elastic range. All the tested specimens deformed within the elastic range and exhibit the same linear behaviour, although there is a large degree of variability in the maximum values of torque applied to twist the torsion specimens.

5.5 Torsional Shear Modulus of the Beams Based on the Data of Inclinometers

Using Equation 1, the shear modulus of the glulam specimens was calculated for each loading-unloading phase in both clockwise and anticlockwise directions and the average value of G was determined by averaging the four measured values of shear modulus from all phases. The calculated shear modulus ranges from 593 to 757 MPa with a mean value of 649 MPa. The difference can be explained by the fact

that inhomogeneity and the variability of the wood specimens, as well as the presence of defects such as knots, affect the overall stiffness of the wood specimens. The average values of shear modulus for each torsion test are very close to each other, although there is a small difference between the values measured in the first two tests and those measured in the last two tests. These results are provided in Fig. 11 which graphically represents the average shear modulus of the test specimens calculated in each trial test. For all torsion specimens, the average values of the shear modulus calculated in the first and second trials are approximately equal, and this is true for those measured from the third and fourth trials. All these values are in good agreement and relatively close to each other with a difference range of 1% to 5%. The shear modulus' values obtained from the first two torsion tests are relatively higher than those obtained from the last two torsion tests.

Table 3 presents the experimental average values of the shear modulus of each specimen calculated from all torsion tests for loading and unloading in both the clockwise and anticlockwise directions. The G_{Avg} indicated in this table represents the average shear modulus of all loading cycles of a test specimen, whereas $G_{Avg\text{-}dir}$ represents the average shear modulus of each loading cycle of all tested specimens. From the loading and unloading cycles, the average values of shear modulus range from 648 to 655 MPa with a consistent standard deviation of (37-39) and a coefficient of variation (COV) of (5.7-6.1%). The small and consistent values of COV may indicate that the torsion test is suitable for determining the shear modulus since the torsion specimen will be under pure torsion.

Fig. 12 demonstrates a graphical representation of the average shear modulus obtained for all glulam beams. In this figure, the average G results for each of the 11 glulam beams (2- 12) listed in Table 3 are compared relative to the average shear modulus of all beams. The overall average G of all the fabricated glulam beams tested in torsion is 649 MPa. This value agrees well with the published value of the same board of glulam beam GL24 and conforms to the requirements of BS EN 14080 (2009).

5.6 Effect of Shear Span on the Variation of Shear Modulus

The torsion specimens were non-destructively evaluated under torsional loading applied within the elastic range. As a result, it becomes essential to examine the effect of span variations on the shear modulus at different cross-sections. Therefore, based on the shape of the photogrammetric patterns, shown in Fig. 13, three shear spans S1, S2, and S3 at the middle section of the torsion specimens were considered. The first shear span, S1, is the distance between sections 1 and 6, representing a gauge length of 1420 mm. The second shear span, S2, is the distance between section 2 and section 5 (the distance between inclinometers B and C), representing a gauge length of 1320 mm and the third shear span, S3, is the distance between section 3 and section 4, representing a gauge length of 1220 mm.

In addition to the stereo images of the photogrammetric patterns, the values of torque were recorded continuously during testing. The relative rotation of each of the two cross-sections over their gauge length (shear span) was measured using the 3D coordinates of the targets distributed on the longer side

of the cross section. Using these data, in addition to the geometry of the torsion specimens, the shear modulus values for each shear span were calculated using Equation (1).

Four torsion tests were conducted on each torsion specimen and the results were averaged. From these results, values of G were obtained for the three shear spans. Table 4 presents the calculated average values of the shear modulus of the three regions of each specimen. The G_{Avg} indicated in this table represents the average shear modulus of all shear spans of a test specimen, whereas $G_{Avg\text{-}span}$ represents the average shear modulus of each shear span of all tested specimens. From Table 4, it can be observed that the average shear modulus varies significantly when considering the three different shear spans of each timber beam.

The largest shear modulus appears to occur at the lowest shear span which is far away from the gripping. On the other hand, the largest span, which is very close to the gripping, attained the smallest shear modulus. The same trend of variation was observed in all test specimens. This result can be clearly observed from the charts plotted in Fig. 14. The values of the shear modulus calculated in the shear span S2 are 10-16% higher than those calculated in the larger span S1 and about 12-17% lower than those calculated in the smaller span S3. For instance, the shear modulus of 613 MPa was attained for shear span S2 of specimen 2 which was 11% higher than the average shear modulus of S1 and 15% lower than the average shear modulus of S3. The main reason for this effect might because the larger span considered in this study is between two sections and one of them is close to the rotating end of the test specimen. The rotation angles affect the shear stiffness and hence the values of shear modulus. The angle of twist in each length is inversely proportional to the shear modulus.

From these results, and within the selected shear spans, it can be concluded that the larger the shear span the smaller the value of shear modulus. The comparison suggests that testing beams in different shear spans are essential to evaluate the variations of the shear modulus values at these different gauge lengths.

5.7 Effects of the Direction of the Applied Torque and Loading Phases on the Values of Shear Modulus

To assess possible misalignment of the test specimens and to observe whether inducing torque in a clockwise or anticlockwise direction influences the torsional behaviour and hence the shear modulus of the specimens, the torsion tests were conducted on each torsion specimen under cyclic loading. Each torsion test consists of phases of torque loading and unloading in a clockwise direction, followed by loading and unloading phases in an anticlockwise direction. From the results of shear modulus presented in Table 3, it can be observed that the experimental values of shear modulus measured for all trial tests conducted on each torsion sample are consistent regardless of the direction of the torque or the loading phases. However, there is a small deviation which is expected for engineered wood products such as glulam beams. As mentioned before, the experimental values of shear modulus are in good agreement and are relatively close to each other with a difference range of 1% to 5%. This may indicate that shear

modulus is less sensitive to torque direction as there was no significant influence of the torque direction on the measured shear modulus.

5.8 Influence of Inverting the Glulam Samples

To investigate the effects of inverting the torsion samples on the torsional behaviour, sample 10 was tested under torsional loads in two ways: the right way up and upside down. Therefore, two names, 10A and 10B, were defined for this specimen to define the right way up and upside down, respectively. Table 5 reports the average shear modulus of this specimen calculated in both orientations. When installing torsion specimens, the right-side up, the average values of shear modulus calculated from the first and second trials are relatively higher than those measured from the third and fourth trials. On the other hand, when inverting specimen 10, the average values of the shear modulus calculated from the first and second trials are relatively smaller than those calculated from the third and fourth trials. It can be concluded that mounting the torsion specimens the right way up during the torsion test yields higher values of shear modulus than those obtained when inverting the specimen, although this finding was based on only a single piece of glulam beam.

Conclusion And Recommendations

5.1 Calibration Results of the Stereo Camera Systems

In order to reconstruct the 3D coordinates of the photogrammetric targets captured by the stereo cameras, and hence determine their rotational deformations, the calibration parameters of the stereo camera systems were determined by performing the binocular stereo camera calibration of each system using the image processing software. This was achieved via a least square solution with suitable chosen parameters of the cameras that can be determined from the specification of the camera sensor and lens. Tables 1 and 2 show selected examples of the internal and external parameters, including the rotation angles and the translation vector determined from the first stereo system. A screenshot of the developed GUI during the process of calibrating the stereo camera system is shown in Fig. 6.

5.2 Target Tracking and 3D Reconstruction

The image processing algorithm is based on the comparison between two images acquired during the test, one before and after deformation. Fig. 7 demonstrates the concept and steps involved in the algorithm. The process starts with reading the calibration files and displaying the stereo images of the targets recorded from the left and right cameras during testing. Based on their shape and size, the potential targets were determined and tracked from the two sequences of stereo images using the sub pixel-precise segmentation method. These targets were fitted to ellipse shapes and their image coordinates in both the left and right images were measured. The 3D coordinates of the targets expressed in the camera coordinates of the left camera were determined using the theory of triangulation [2]. These coordinates were then used in the calculation of the displacements and rotations of the targets during the period of tests. This was achieved by finding the pixel coordinates of the targets of each pattern and

averaging these values to define a point with the average pixel coordinates of the pattern. The pixel coordinates of the other two points were determined for each pair of the stereo images by processing the initial images before applying torque to the specimens. Utilizing the calibration parameters of the stereo camera system and triangulation, the 3D coordinates of the three points were determined to define two vectors. Using the two vectors, the rotations of the photogrammetric patterns for each time interval were then calculated.

5.3 Comparison of Angular Deformations Measured by Inclinometers and the Photogrammetric Systems

To understand the differences between the rotations of the long and short sides of the cross section, the rotations of photogrammetric patterns 1 and 2 and the rotations of inclinometers B and C were plotted in the same figure. These data were measured in both clockwise and anticlockwise directions under torque loading and unloading phases. Fig. 8 (a) and (b) show some selected examples of these comparisons and indicate remarkable results. It is evident that a good agreement between the two methods has been observed and this indicates that the measurements of the rotations of the short side with inclinometers are acceptable.

To investigate the correlation between the measurements, the rotation results of the inclinometers and stereo camera systems were plotted against each other and a very strong correlation was observed for each glulam timber specimen. Selected examples of this comparison are shown in Fig. 9 (a) and (b) in which the rotations of specimen 4, measured in the torsional direction by inclinometers B and C and by the first and second binocular stereo systems, were plotted against each other. These figures provide further evidence of this correlation when considering the correlation of determination (R^2) of the angular measurements of inclinometers versus stereo camera systems. From the results shown in these figures a high degree of correlation, with an R-squared value of 0.999, was observed.

5.4 Torsional Behaviour of the Glulam Timber Beams

The results of preliminary tests that were carried out on specimen 1 revealed that the maximum torque applied to the specimen was within the linear-elastic range, about 250 N.m, and the torsion specimen could be twisted by up to 15° before it began to behave non-linearly. This result was found from the inclinometers which were mounted near the reactional supports. Based on this finding, torsion tests were conducted four times on each of the remaining eleven specimens (2-12) under cyclic loading in the clockwise and anticlockwise directions. The recorded torques measured from the torque cell of the torsion machine, were analyses and displayed graphically. As an example, the torque versus time graph obtained from the first torsion test conducted on glulam specimen 2 under loading and unloading phases is shown in Fig. 10. This plot indicates that the relationship between the values of torque and the

corresponding time is approximately linear during the different phases of loadings, confirming that the torsion specimen was within the elastic range. All the tested specimens deformed within the elastic range and exhibit the same linear behaviour, although there is a large degree of variability in the maximum values of torque applied to twist the torsion specimens.

5.5 Torsional Shear Modulus of the Beams Based on the Data of Inclinometers

Using Equation 1, the shear modulus of the glulam specimens was calculated for each loading-unloading phase in both clockwise and anticlockwise directions and the average value of G was determined by averaging the four measured values of shear modulus from all phases. The calculated shear modulus ranges from 593 to 757 MPa with a mean value of 649 MPa. The difference can be explained by the fact that inhomogeneity and the variability of the wood specimens, as well as the presence of defects such as knots, affect the overall stiffness of the wood specimens. The average values of shear modulus for each torsion test are very close to each other, although there is a small difference between the values measured in the first two tests and those measured in the last two tests. These results are provided in Fig. 11 which graphically represents the average shear modulus of the test specimens calculated in each trial test. For all torsion specimens, the average values of the shear modulus calculated in the first and second trials are approximately equal, and this is true for those measured from the third and fourth trials. All these values are in good agreement and relatively close to each other with a difference range of 1% to 5%. The shear modulus' values obtained from the first two torsion tests are relatively higher than those obtained from the last two torsion tests.

Table 3 presents the experimental average values of the shear modulus of each specimen calculated from all torsion tests for loading and unloading in both the clockwise and anticlockwise directions. The G_{Avg} indicated in this table represents the average shear modulus of all loading cycles of a test specimen, whereas $G_{Avg\text{-}dir}$ represents the average shear modulus of each loading cycle of all tested specimens. From the loading and unloading cycles, the average values of shear modulus range from 648 to 655 MPa with a consistent standard deviation of (37-39) and a coefficient of variation (COV) of (5.7-6.1%). The small and consistent values of COV may indicate that the torsion test is suitable for determining the shear modulus since the torsion specimen will be under pure torsion.

Fig. 12 demonstrates a graphical representation of the average shear modulus obtained for all glulam beams. In this figure, the average G results for each of the 11 glulam beams (2- 12) listed in Table 3 are compared relative to the average shear modulus of all beams. The overall average G of all the fabricated glulam beams tested in torsion is 649 MPa. This value agrees well with the published value of the same board of glulam beam GL24 and conforms to the requirements of BS EN 14080 (2009).

5.6 Effect of Shear Span on the Variation of Shear Modulus

The torsion specimens were non-destructively evaluated under torsional loading applied within the elastic range. As a result, it becomes essential to examine the effect of span variations on the shear modulus at different cross-sections. Therefore, based on the shape of the photogrammetric patterns, shown in Fig.

13, three shear spans S1, S2, and S3 at the middle section of the torsion specimens were considered. The first shear span, S1, is the distance between sections 1 and 6, representing a gauge length of 1420 mm. The second shear span, S2, is the distance between section 2 and section 5 (the distance between inclinometers B and C), representing a gauge length of 1320 mm and the third shear span, S3, is the distance between section 3 and section 4, representing a gauge length of 1220 mm.

In addition to the stereo images of the photogrammetric patterns, the values of torque were recorded continuously during testing. The relative rotation of each of the two cross-sections over their gauge length (shear span) was measured using the 3D coordinates of the targets distributed on the longer side of the cross section. Using these data, in addition to the geometry of the torsion specimens, the shear modulus values for each shear span were calculated using Equation (1).

Four torsion tests were conducted on each torsion specimen and the results were averaged. From these results, values of G were obtained for the three shear spans. Table 4 presents the calculated average values of the shear modulus of the three regions of each specimen. The G_{Avg} indicated in this table represents the average shear modulus of all shear spans of a test specimen, whereas $G_{Avg\text{-}span}$ represents the average shear modulus of each shear span of all tested specimens. From Table 4, it can be observed that the average shear modulus varies significantly when considering the three different shear spans of each timber beam.

The largest shear modulus appears to occur at the lowest shear span which is far away from the gripping. On the other hand, the largest span, which is very close to the gripping, attained the smallest shear modulus. The same trend of variation was observed in all test specimens. This result can be clearly observed from the charts plotted in Fig. 14. The values of the shear modulus calculated in the shear span S2 are 10-16% higher than those calculated in the larger span S1 and about 12-17% lower than those calculated in the smaller span S3. For instance, the shear modulus of 613 MPa was attained for shear span S2 of specimen 2 which was 11% higher than the average shear modulus of S1 and 15% lower than the average shear modulus of S3. The main reason for this effect might because the larger span considered in this study is between two sections and one of them is close to the rotating end of the test specimen. The rotation angles affect the shear stiffness and hence the values of shear modulus. The angle of twist in each length is inversely proportional to the shear modulus.

From these results, and within the selected shear spans, it can be concluded that the larger the shear span the smaller the value of shear modulus. The comparison suggests that testing beams in different shear spans are essential to evaluate the variations of the shear modulus values at these different gauge lengths.

5.7 Effects of the Direction of the Applied Torque and Loading Phases on the Values of Shear Modulus

To assess possible misalignment of the test specimens and to observe whether inducing torque in a clockwise or anticlockwise direction influences the torsional behaviour and hence the shear modulus of

the specimens, the torsion tests were conducted on each torsion specimen under cyclic loading. Each torsion test consists of phases of torque loading and unloading in a clockwise direction, followed by loading and unloading phases in an anticlockwise direction. From the results of shear modulus presented in Table 3, it can be observed that the experimental values of shear modulus measured for all trial tests conducted on each torsion sample are consistent regardless of the direction of the torque or the loading phases. However, there is a small deviation which is expected for engineered wood products such as glulam beams. As mentioned before, the experimental values of shear modulus are in good agreement and are relatively close to each other with a difference range of 1% to 5%. This may indicate that shear modulus is less sensitive to torque direction as there was no significant influence of the torque direction on the measured shear modulus.

5.8 Influence of Inverting the Glulam Samples

To investigate the effects of inverting the torsion samples on the torsional behaviour, sample 10 was tested under torsional loads in two ways: the right way up and upside down. Therefore, two names, 10A and 10B, were defined for this specimen to define the right way up and upside down, respectively. Table 5 reports the average shear modulus of this specimen calculated in both orientations. When installing torsion specimens, the right-side up, the average values of shear modulus calculated from the first and second trials are relatively higher than those measured from the third and fourth trials. On the other hand, when inverting specimen 10, the average values of the shear modulus calculated from the first and second trials are relatively smaller than those calculated from the third and fourth trials. It can be concluded that mounting the torsion specimens the right way up during the torsion test yields higher values of shear modulus than those obtained when inverting the specimen, although this finding was based on only a single piece of glulam beam.

Declarations

Acknowledgements

The authors would like to express their special gratitude to the financial support of the National Nature Science Foundation of China (51768008), British Council and Ministry of Education, China (UK-China-BRI Countries Education Partnership Initiative 2019), China Postdoctoral Science Foundation Project (2017M613273XB), Liuzhou Scientific Research and Technology Development Plan (2017BC40202), Lawrence Ho Research Fund, Royal Academy of Engineering – Visiting Professor (VP2021\7\12) and Royal Academy of Engineering – Industrial Fellowship (IF\192023). The authors also acknowledge the support of Innovation Team Support Plan of Guangxi University of Science and Technology.

Competing interests: The authors declare no competing interests.

References

Choi, D., et al. (1991). Image analysis to measure strain in wood and paper. *Wood Science and Technology* **25**(4): 251-262.

Chui, Y. (2002). Application of ribbed-plate theory of predict vibrational serviceability of timber floor systems. *The Proceedings of 7 th World Conference on Timber Engineering WCTE*, Vol **4**: 87-93.

Dahl, K. and K. Malo (2009). Planar strain measurements on wood specimens. *Experimental mechanics* **49**(4): 575-586.

Dahl, K. B. and K. Malo (2009). Linear shear properties of spruce softwood. *Wood Science and Technology* **43**(5-6): 499-525.

Dahl, K. B. and K. Malo (2009). Nonlinear shear properties of spruce softwood: experimental results. *Wood Science and Technology* **43**(7-8): 539-558.

EN 338:2009 (2009). *Structural Timber - Strength Classes*. European Committee for Standardization, Brussels, Belgium.

EN 408:2012 (2012). *Timber structures-structural timber and glued laminated timber- determination of some physical and mechanical properties perpendicular to the grain*. European Committee for Standardization, Brussels, Belgium.

EN 1995-1-1 (2004). *Eurocode 5-Design of Timber Structures-Part 1-1: General-Common Rules and Rules for Buildings*. European Committee for Standardization, Brussels, Belgium.

Foschi, R. O. (1982). Structural analysis of wood floor systems. *Journal of the Structural Division* **108**(7): 1557-1574.

Franke, S., et al. (2007). Strain analysis of wood components by close range photogrammetry. *Materials and structures* **40**(1): 37-46.

Garcia, D. and J.-J. Orteu (2001). 3D deformation measurement using stereo-correlation applied to experimental mechanics. *Proceedings of the 10th International Symposium Deformation Measurements*.

Gharavi, N. and Zhang, H., 2018. Study on the Impact of Size and Position of the Shear Field in Determining the Shear Modulus of Glulam Beam Using Photogrammetry Approach. World Academy of Science, Engineering and Technology, *International Journal of Structural and Construction Engineering*, 12(3), pp.218-222. doi.org/10.5281/zenodo.1315953

Gharavi N, Zhang H, Xie Y., 2017. Evaluation of the end effect impact on the torsion test for determining the shear modulus of a timber beam through a photogrammetry approach. World Academy of Science, Engineering and Technology, *International Journal of Mechanical and Mechatronics Engineering*, 11(3):677–680. doi.org/10.5281/zenodo.1129778

Gharavi, N., Zhang, H., Xie, Y. and He, T. (2018). End effect on determining shear modulus of timber beams in torsion test, *Construction and Building Materials*, 164:442-450.

Guindos, P. and J. Ortiz (2013). Low cost photogrammetry as a tool for stiffness analysis and finite element validation of timber with knots in bending, *Biosystems Engineering*, 114(2): 86-96.

Gupta, R., et al. (2002). Experimental evaluation of the torsion test for determining shear strength of structural lumber. *Journal of testing and evaluation* **30** (4): 283-290.

Gupta, R., Siller, Tobias (2005). Shear strength of structural composite lumber using torsion tests. *Journal of testing and evaluation* **33** (2): 110-117.

Hartley, R. and A. Zisserman (2003). Multiple view geometry in computer vision, *Cambridge university press*.

Hindman, D., et al. (2005a). Torsional rigidity of rectangular wood composite materials. *Wood and fiber science* **37** (2): 283-291.

Hindman, D., et al. (2005b). Torsional rigidity of wood composite I-joists. *Wood and fiber science* **37** (2): 292-303.

Jiang, L., et al. (2004). Finite-element model for wood-based floors with lateral reinforcements. *Journal of Structural Engineering* **130**(7): 1097-1107.

Khokhar, A., et al. (2010). The shear strength, and failure modes, of timber joists obtained from the torsion test method. *Proceedings of the 11th World Conference of Timber Engineering*, 20-24th June, Riva del Garda, Italy.

Khokhar, A. M. (2011). The Evaluation of Shear Properties of Timber Beams Using Torsion Test Method. *PhD Thesis*, Edinburgh Napier University, Edinburgh, UK.

Maas, H.-G. and U. Hampel (2006). Photogrammetric techniques in civil engineering material testing and structure monitoring. *Photogrammetric Engineering & Remote Sensing* **72**(1): 39-45.

MVTech Software HALCON GmbH (2019). The software for Machine Vision Applications. http:// www.mvtech.com/halcon/.

Steger, C., et al. (2008). Machine vision algorithms and applications. *Handbook of machine vision*, Wiley-VCH, Weinheim.

Xavier, J., et al. (2012). Stereovision measurements on evaluating the modulus of elasticity of wood by compression tests parallel to the grain. *Construction and Building Materials* **26**(1): 207-215.

Zhang, H., et al. (2011). Evaluation of shear constant of a timber beam using a photogrammetric approach. *Proceedings of the Thirteenth International Conference on Civil, Structural and Environmental*

Engineering Computing. Crete, Greece.

Zhang, H., et al. (2012). Evaluation of shear constant of timber glulam composite with photogrammetric approach. *Proceedings of the Fourteenth International Conference on Computing in Civil and Building Engineering*, Moscow, Russia.

Tables

Table 1: Internal camera parameters of the first stereo camera system.

Camera Parameter	Description	Unit	Left Camera	Right Camera
Focus	Focal length of the lens	m	0.035	0.035
Kappa	Radial distortion coefficient	m^{-2}	31.57	-14.16
Sx	Width of a cell on the CCD-chip	m	2.2e-006	2.2e-006
Sy	Height of a cell on the CCD-chip	m	2.2e-006	2.2e-006
Cx	X-coordinate of the image centre	Pixels	1503.89	1424.04
Cy	Y-coordinate of the image centre	Pixels	957.12	992.70
Image Width	Width of the images	Pixels	2592	2592
Image Height	Height of the images	Pixels	1944	1944

Table 2: 3D pose parameters (rotation and translation).

Translation vector (X Y Z [m])	X	0.175
	Y	-0.008
	Z	0.000
Rotation angles [degree]	Rot(X)	359.68
	Rot(Y)	355.53
	Rot(Z)	359.16

Table 3: Average shear modulus of each of the torsion samples in all trial tests.

	Average Shear modulus (MPa)				
	Clockwise direction		Anticlockwise direction		
Specimen	Loading	Unloading	Loading	Unloading	G_{Avg}
HT002	656	661	659	659	659
HT003	639	640	636	640	639
HT004	686	687	678	676	682
HT005	656	661	655	656	657
HT006	740	746	743	738	742
HT007	615	618	616	614	616
HT008	669	672	661	662	666
HT009	612	616	608	617	613
HT010	619	623	612	613	617
HT011	621	625	614	618	620
HT012	653	656	649	653	653
$G_{Avg\text{-}dir}$	651	655	648	650	649
Std	38	38	39	37	
COV	5.8	5.9	6.1	5.7	

Table 4: The shear modulus values of three spans of torsion specimens.

Average Shear Modulus (MPa)

Specimen ID	Shear Span			G_{Avg}
	S1	S2	S3	
HT002	547	613	718	**626**
HT003	568	667	745	**660**
HT004	562	667	745	**658**
HT005	568	633	745	**649**
HT006	630	720	803	**718**
HT007	544	624	730	**633**
HT008	571	667	799	**679**
HT009	521	578	659	**586**
HT010A	495	561	651	**569**
HT010B	535	608	717	**620**
HT011	541	624	740	**635**
HT012	515	569	656	**580**
$G_{avg\text{-}span}$	**550**	**628**	**726**	**634**

Figures

Figure 1

Glulam beam samples before and after photogrammetric patterns painted.

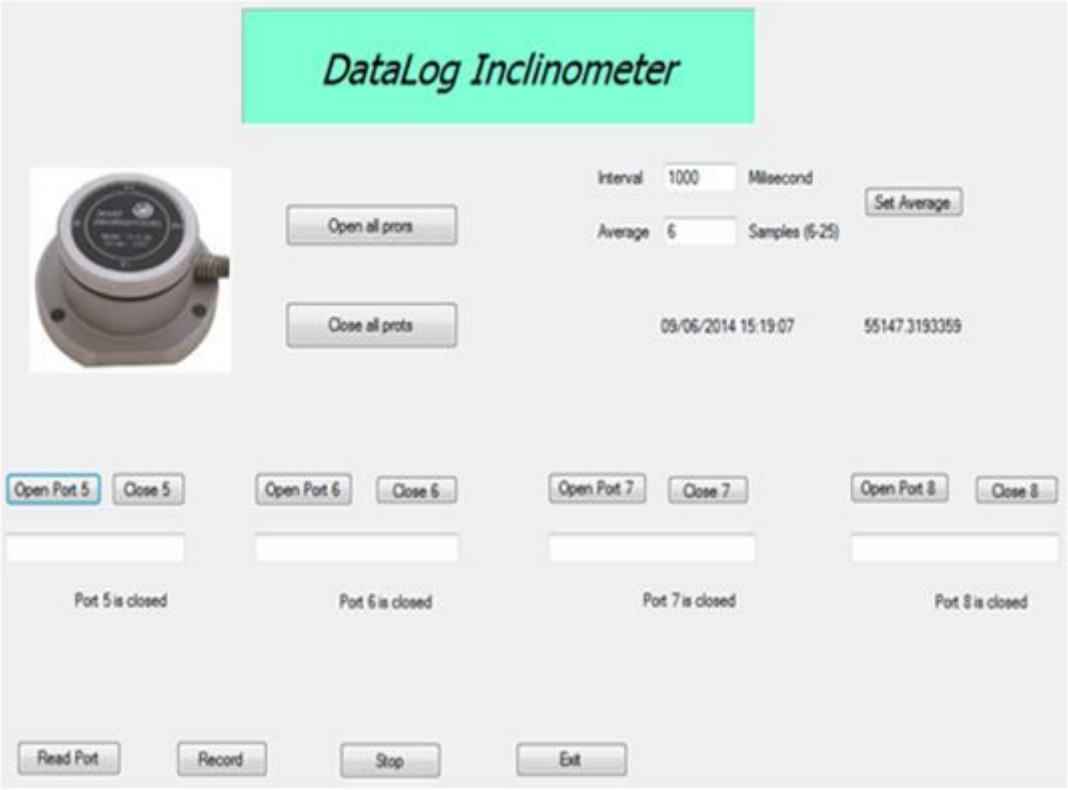

Figure 2

The Purpose-built dual-axis inclinometer Data Log System.

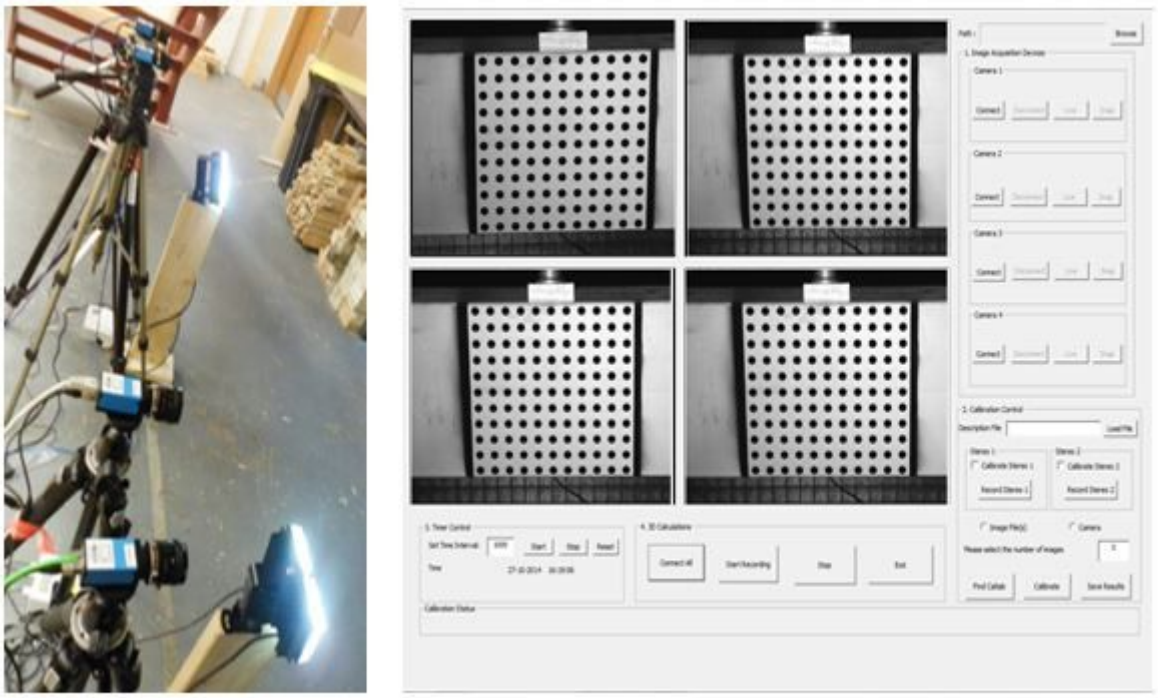

(a) (b)

Figure 3

(a) The binocular stereo camera systems, (b) Screen shot of purpose-built photogrammetric software.

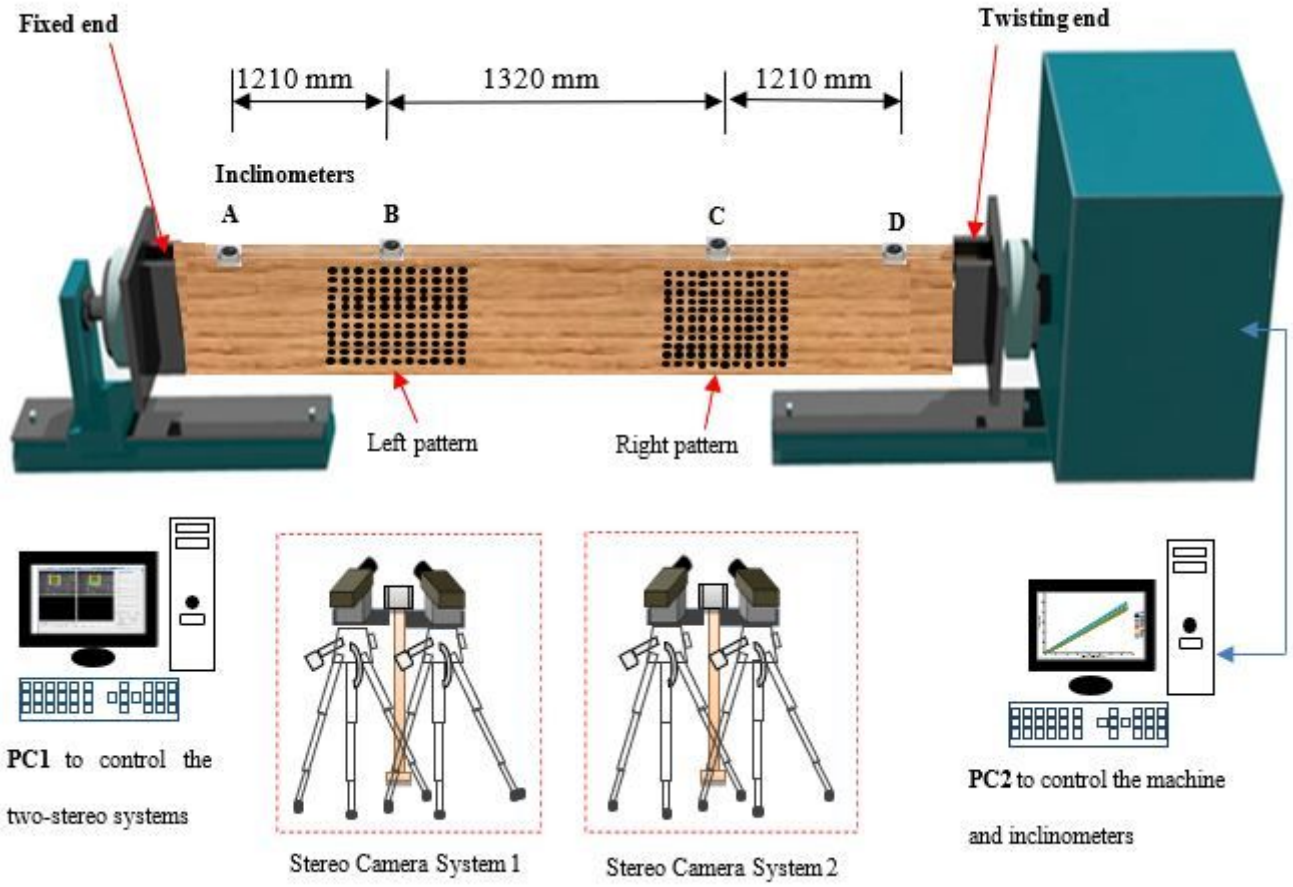

Figure 4

Torsion test and dual stereo vision cameras setup.

Figure 5

Lab photo of Torsion test and dual stereo vision cameras setup.

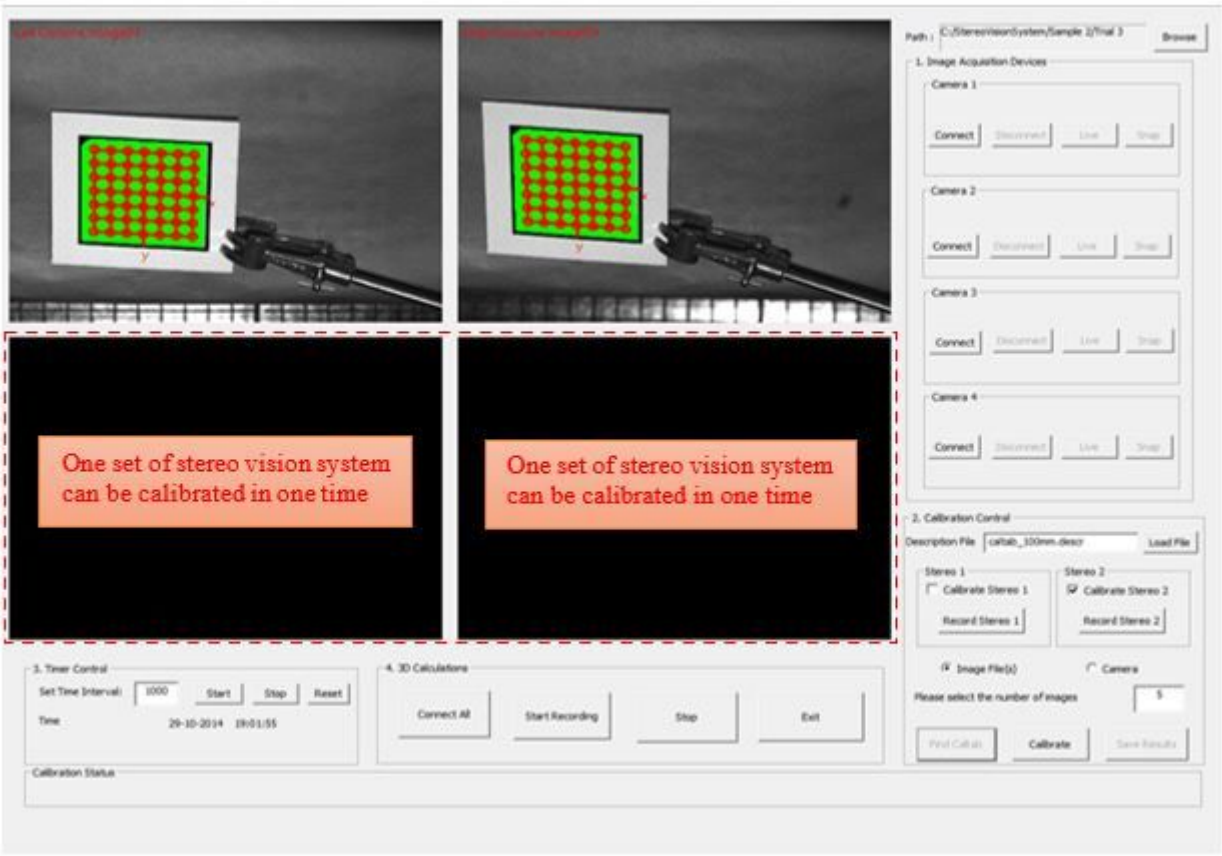

Figure 6

Calibration of the stereo vision system.

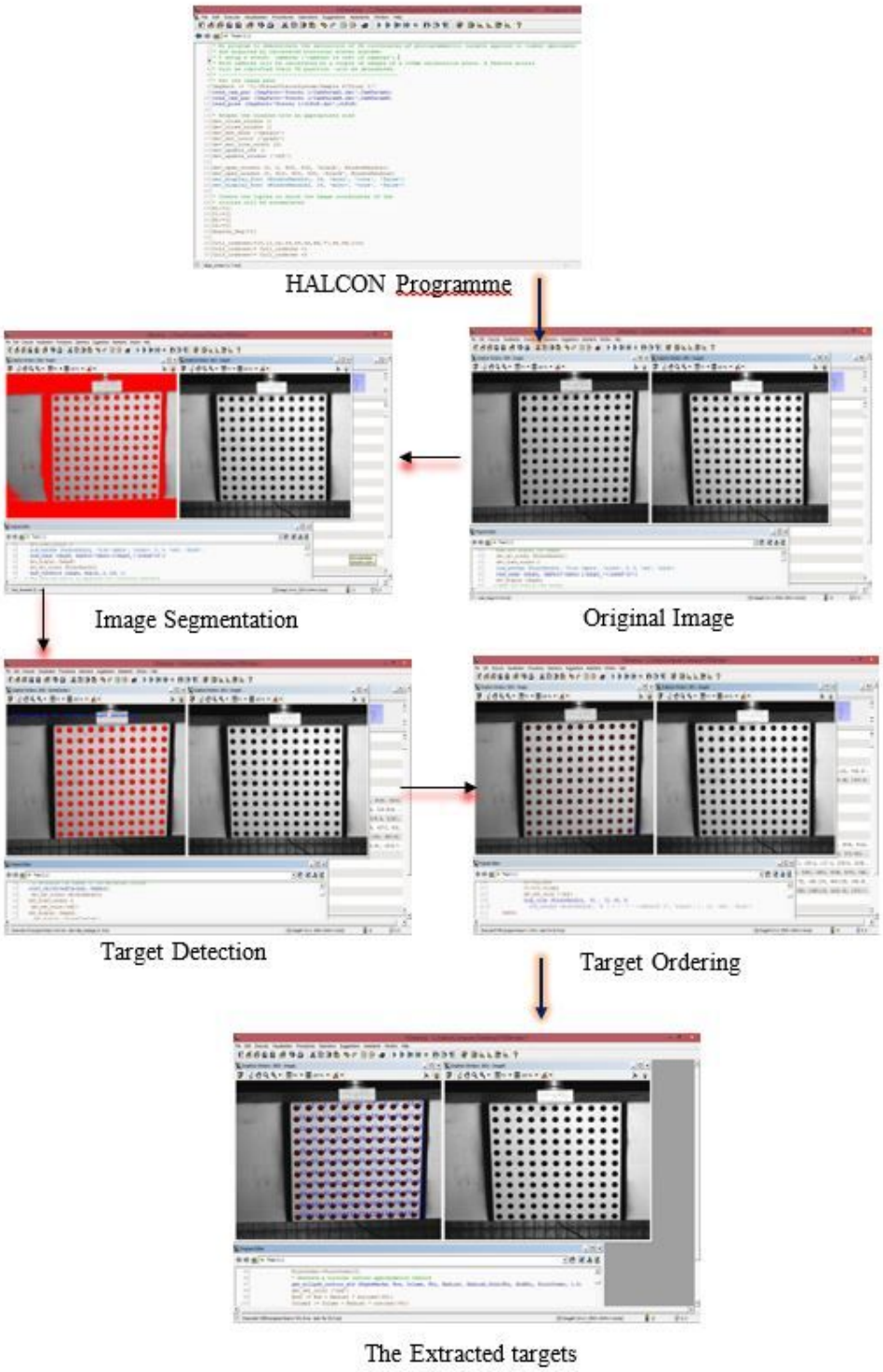

1

Figure 7

Indicative flowchart for photogrammetric measurement.

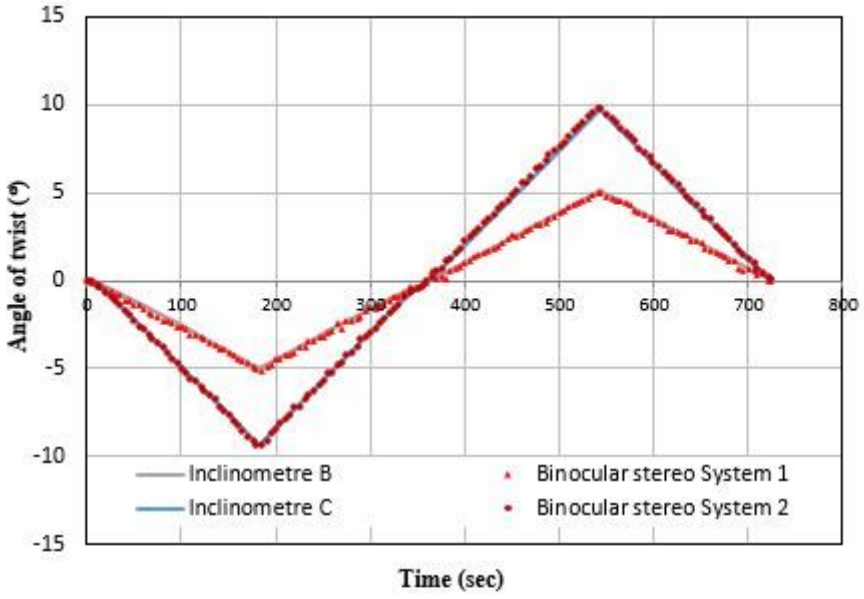

(a)

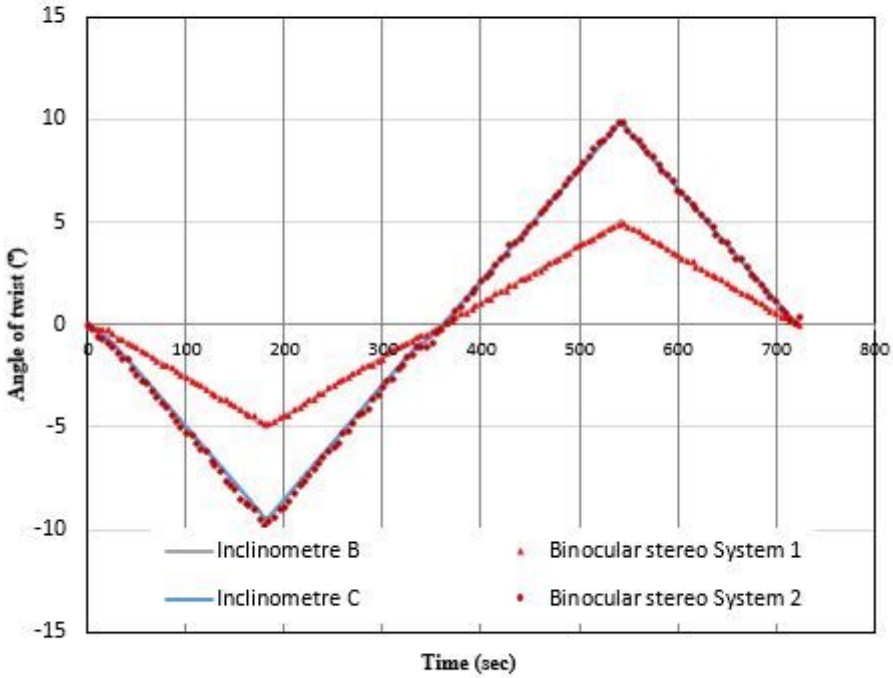

(b)

Figure 8

Comparison between inclinometers and optical measurements for (a) sample 5, and (b) sample 9 in the first torsion test.

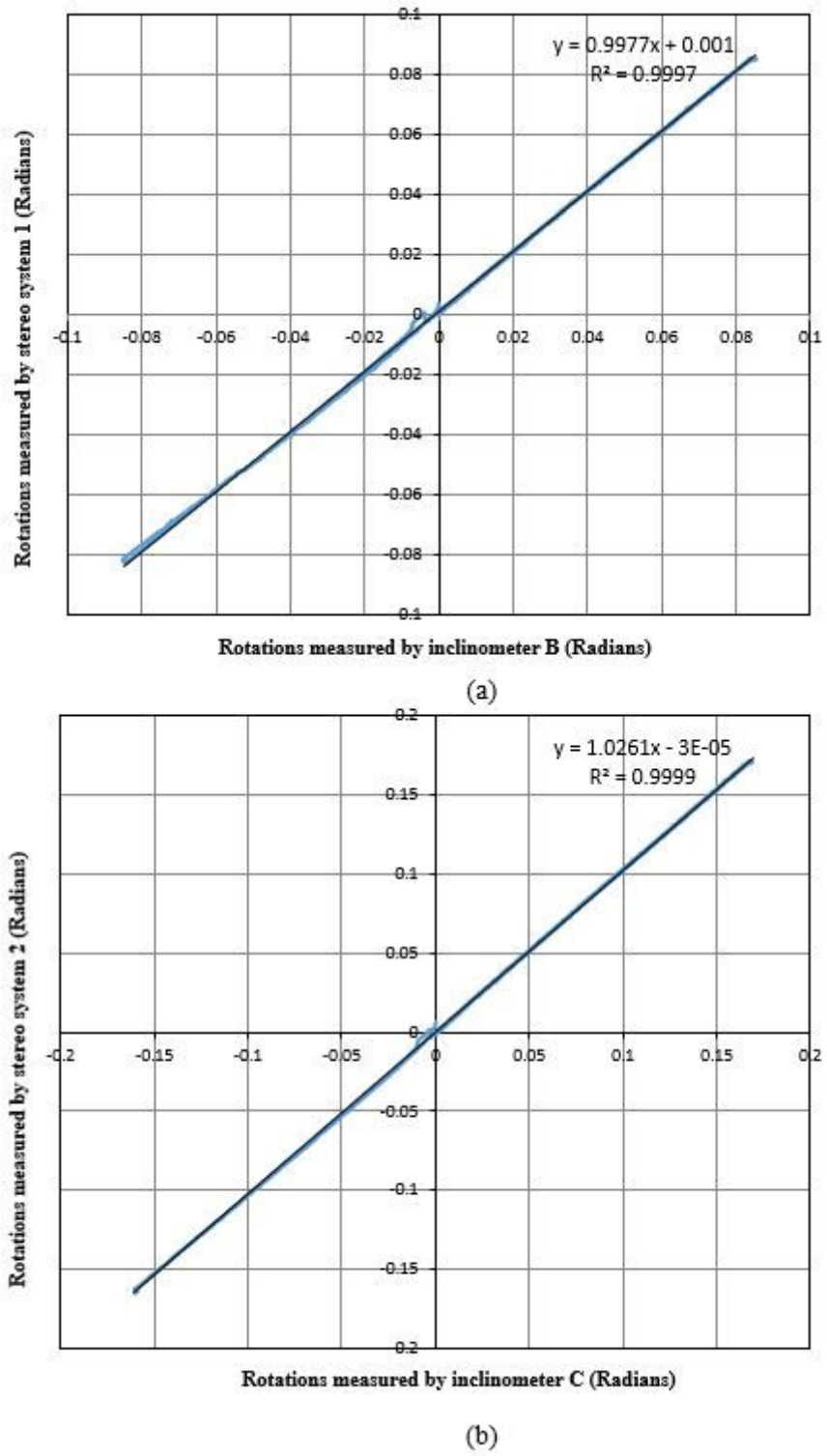

Figure 9

Comparison of the rotations measured in specimen 4 between (a) inclinometer B and the stereo camera system 1, and (b) inclinometer C and the stereo camera system 2.

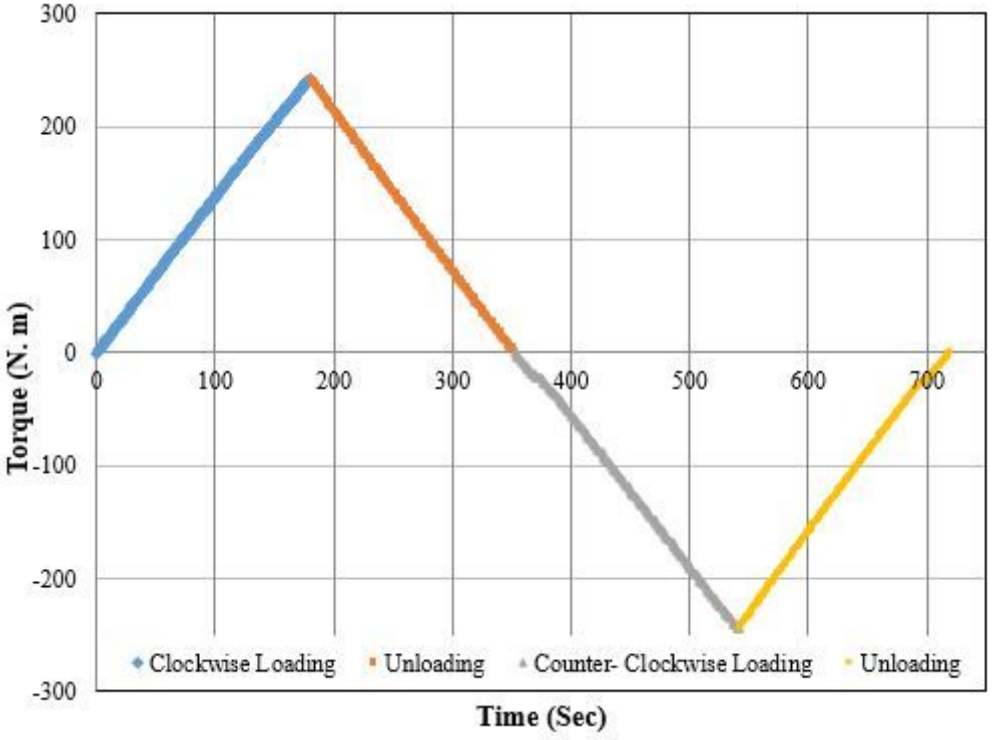

Figure 10

Responses of sample 2 to torques during the four phases of loading in the first torsion test.

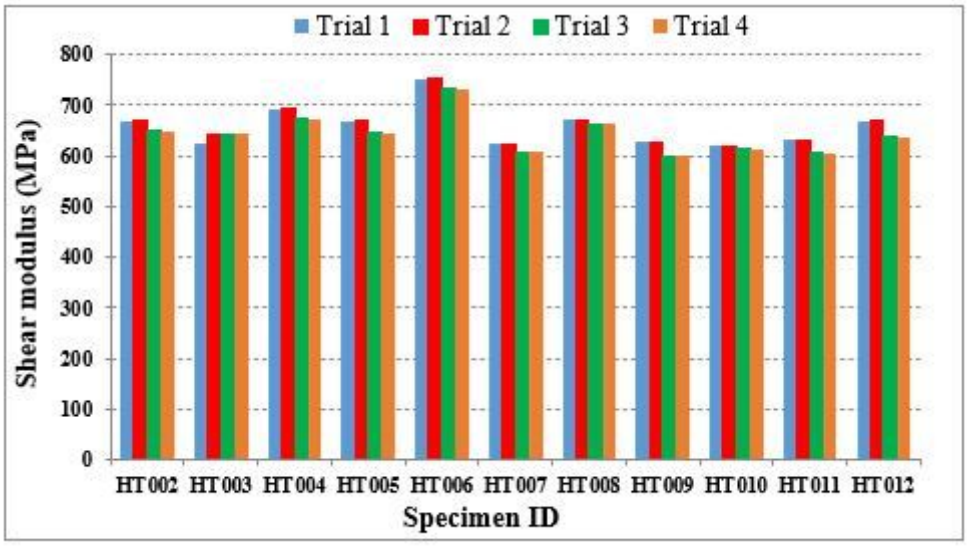

Figure 11

The average shear modulus of the torsion specimens calculated from each torsion test.

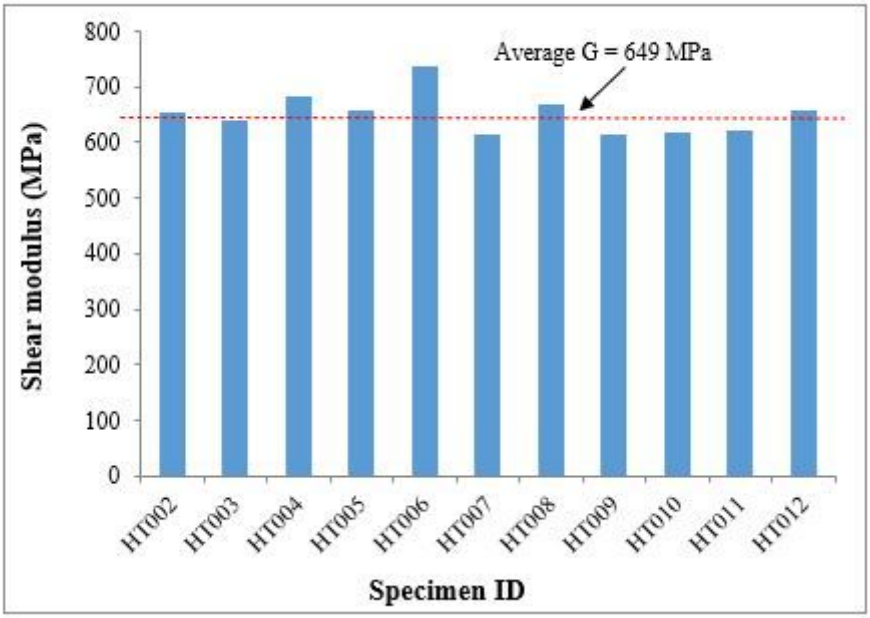

Figure 12

The average shear modulus of the torsion specimens.

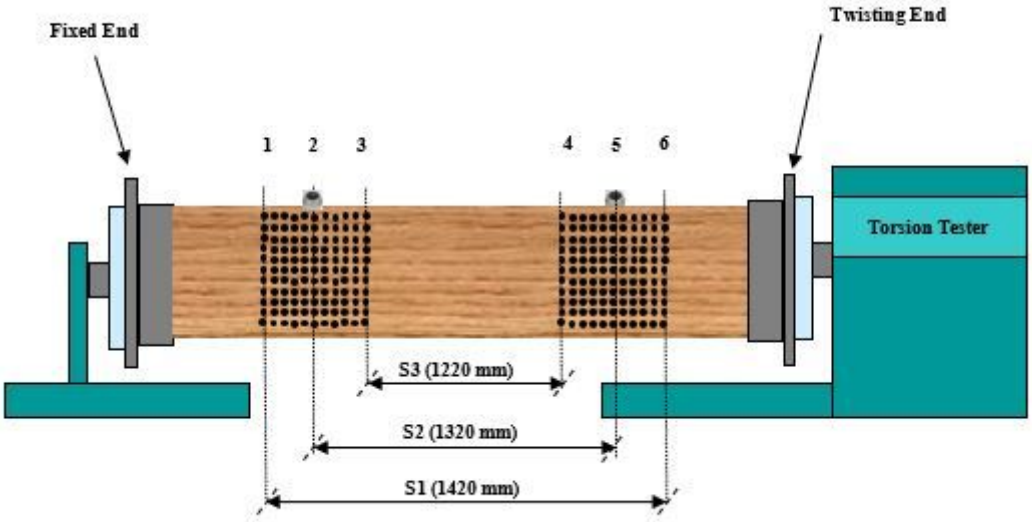

Figure 13

Diagram of the different shear spans for determining the shear modulus on various segments.

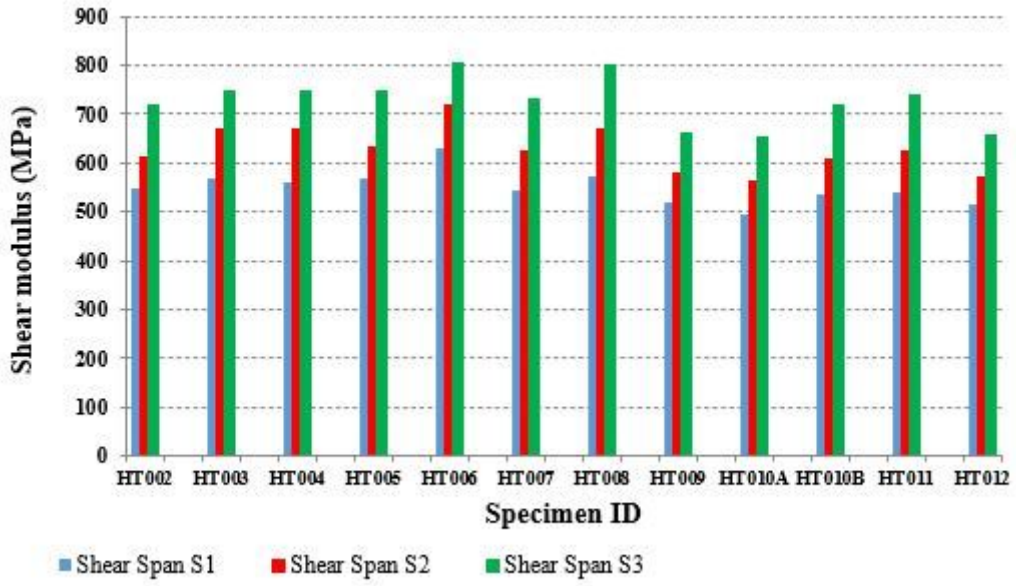

Figure 14

Variations of shear modulus at different shear spans.

Supplementary Files

This is a list of supplementary files associated with this preprint. Click to download.

- formula.docx